Springer Handbook of Materials Measurement Methods

Horst Czichos, Tetsuya Saito, Leslie Smith (Eds.)

With CD-ROM, 970 Figures and 158 Tables

Editors:
Horst Czichos
Federal Institute for Materials Research
and Testing (BAM), Past President;
University of Applied Sciences Berlin
Germany

Tetsuya Saito
National Institute for Materials Science (NIMS)
Tsukuba, Ibaraki
Japan

Leslie Smith
National Institute of Standards and Technology (NIST)
Gaithersburg, MD
USA

Library of Congress Control Number: 2006921595

ISBN-10: 3-540-20785-6
ISBN-13: 978-3-540-20785-6
e-ISBN: 3-540-30300-6
Printed on acid free paper

© 2006, Springer Science+Business Media, Inc.
All rights reserved. This work may not be translated or copied in whole or in part without the written permission of the publisher (Springer Science+ Business Media, Inc., 233 Spring Street, New York, NY 10013, USA), except for brief excerpts in connection with reviews or scholarly analysis. Use in connection with any form of information storage and retrieval, electronic adaptation, computer software, or by similar or dissimilar methodology now known or hereafter developed is forbidden. The use in this publication of trade names, trademarks, service marks, and similar terms, even if they are not identified as such, is not to be taken as an expression of opinion as to whether or not they are subject to proprietary rights.

The use of designations, trademarks, etc. in this publication does not imply, even in the absence of a specific statement, that such names are exempt from the relevant protective laws and regulations and therefore free for general use.

Product liability: The publisher cannot guarantee the accuracy of any information about dosage and application contained in this book. In every individual case the user must check such information by consulting the relevant literature.

Production and typesetting: LE-TeX GbR, Leipzig
Handbook coordinator: Dr. W. Skolaut, Heidelberg
Typography, layout and illustrations:
schreiberVIS, Seeheim & Hippmann GbR, Schwarzenbruck
Cover design: eStudio Calamar Steinen, Barcelona
Cover production: WMXDesign GmbH, Heidelberg
Printing and binding: Stürtz AG, Würzburg

SPIN 10918104 62/3141/YL 5 4 3 2 1 0

8.2 Enthalpy of Phase Transition, Adsorption and Mixing 408
8.2.1 Adiabatic Calorimetry 409
8.2.2 Differential Scanning Calorimetry 411
8.2.3 Drop Calorimetry 412
8.2.4 Solution Calorimetry 413
8.2.5 Combustion Calorimetry 414
8.3 Thermal Expansion and Thermomechanical Analysis 415
8.3.1 Optical Methods 415
8.3.2 Push Rod Dilatometry 416
8.3.3 Thermomechanical Analysis 416
8.4 Thermogravimetry 417
8.5 Temperature Sensors 417
8.5.1 Temperature and Temperature Scale 417
8.5.2 Use of Thermometers 420
8.5.3 Resistance Thermometers 421
8.5.4 Liquid-in-Glass Thermometers 423
8.5.5 Thermocouples 424
8.5.6 Radiation Thermometers 425
8.5.7 Cryogenic Temperature Sensors 426
References 428

9 **Electrical Properties**
Bernd Schumacher, Heinz-Gunter Bach, Petra Spitzer, Jan Obrzut 431
9.1 Electrical Materials 432
9.1.1 Conductivity and Resistivity of Metals 432
9.1.2 Superconductivity 433
9.1.3 Semiconductors 434
9.1.4 Conduction in Polymers 435
9.1.5 Ionic Conductors 436
9.1.6 Dielectricity 437
9.1.7 Ferroelectricity and Piezoelectricity 438
9.2 Electrical Conductivity of Metallic Materials 439
9.2.1 Scale of Electrical Conductivity; Reference Materials 439
9.2.2 Principal Methods 440
9.2.3 DC Conductivity, Calibration of Reference Materials 441
9.2.4 AC Conductivity, Calibration of Reference Materials 442
9.2.5 Superconductivity 443
9.3 Electrolytical Conductivity 444
9.3.1 Scale of Conductivity 445
9.3.2 Basic Methods 445
9.3.3 The Measurement of the Electrolytic Conductivity 447
9.4 Semiconductors 453
9.4.1 Conductivity Measurements 453
9.4.2 Mobility Measurements 456
9.4.3 Dopant and Carrier Concentration Measurements 459
9.4.4 *I–V* Breakdown Mechanisms 463
9.4.5 Deep Level Characterization and Minority Carrier Lifetime . 465

9.4.6 Contact Resistances of Metal-Semiconductor Contacts 469
9.5 Measurement of Dielectric Materials Properties 472
9.5.1 Dielectric Permittivity 473
9.5.2 Measurement of Permittivity 475
9.5.3 Uncertainty Considerations 480
9.5.4 Conclusion 481
References 481

10 **Magnetic Properties**
Joachim Wecker, Günther Bayreuther, Gunnar Ross, Roland Grössinger 485
10.1 Magnetic Materials 486
10.1.1 Diamagnetism, Paramagnetism, and Ferromagnetism 486
10.1.2 Antiferromagnetism and Ferrimagnetism 487
10.1.3 Intrinsic and Extrinsic Properties 487
10.1.4 Bulk Soft and Hard Materials 488
10.1.5 Magnetic Thin Films 488
10.1.6 Time-Dependent Changes in Magnetic Properties 489
10.1.7 Definition of Magnetic Properties and Respective Measurement Methods 489
10.2 Soft and Hard Magnetic Materials: (Standard) Measurement Techniques for Properties Related to the $B(H)$ Loop 490
10.2.1 Introduction 490
10.2.2 Properties of Hard Magnetic Materials 493
10.2.3 Properties of Soft Magnetic Materials 499
10.3 Magnetic Characterization in a Pulsed Field Magnetometer (PFM) 510
10.3.1 Industrial Pulsed Field Magnetometer 510
10.3.2 Errors in a PFM 512
10.3.3 Calibration 516
10.3.4 Hysteresis Measurements on Hard Magnetic Materials 518
10.3.5 Anisotropy Measurement 519
10.3.6 Summary: Advantages and Disadvantages of PFM 521
10.4 Properties of Magnetic Thin Films 522
10.4.1 Saturation Magnetization, Spontaneous Magnetization 522
10.4.2 Magneto-Resistive Effects 526
References 527

11 **Optical Properties**
Tadashi Itoh, Tsutomu Araki, Masaaki Ashida, Tetsuo Iwata, Kiyofumi Muro, Noboru Yamada 531
11.1 Fundamentals of Optical Spectroscopy 532
11.1.1 Light Source 532
11.1.2 Photosensors 534
11.1.3 Wavelength Selection 536
11.1.4 Reflection and Absorption 538
11.1.5 Luminescence and Lasers 542
11.1.6 Scattering 546

Detailed Cont.

From these two voltage values V_1 and V_2 together with the constant current I the sheet resistance R_s and the total contact resistance R_c under each contact can be calculated by

$$R_s = \frac{V_1 - V_2}{l_1 - l_2} \frac{w}{I} ,$$

and

$$R_c = \frac{1}{2}\left(\frac{V_1}{I} - l_1 \frac{R_s}{w}\right) . \quad (9.67)$$

With these two terms now (9.66) can be used to extract the specific contact resistance ρ_c. The contact distances l_1 and l_2 (1–100 μm) need to be determined with high precision (sub-micron range) because otherwise larger errors would result for ρ_c, especially when ρ_c falls below $10^{-6}\,\Omega\,cm^2$.

For electrically long contacts (e.g. $d = 40\,\mu m$) the transfer length L_T is defined as $L_T = \sqrt{\rho_c/R_s}$. The transfer length illustrates the typical length for the current to pass from the epitaxial layer into the metal contact. Practical contacts do not need to be designed longer than about three transfer lengths.

The transfer resistance R_T is defined as $R_T = \sqrt{R_s \rho_c}$ (Ω mm). The transfer resistance characterizes the lowest contact resistance which can be achieved for an electrically long contact of a given width w. Transfer resistance values for e.g. FETs should be lower than 0.2 Ω mm.

9.5 Measurement of Dielectric Materials Properties

Dielectric materials are the building blocks of functional electronic circuits, capacitors, gate dielectrics, transmission lines are essential as electrical insulators for power distribution. Molecular solids, organic polymer resins, ceramic glasses and composites of organic resins with ceramic fillers represent typical dielectrics. The dielectric properties of materials are used to describe electrical energy storage, dissipation and energy transfer. Electrical storage is the result *dielectric polarization*. Dielectric polarization causes charge displacement or rearrangement of molecular dipoles. Electrical energy dissipation or *loss* results from (1) electrical charge transport or *conduction*, (2) *dielectric relaxation*, (3) *resonant transitions* and (4) *nonlinear dielectric* effects. Energy loss is eventually related to scattering, radiation or conversion of electrical energy into thermal energy (Joule heating). Energy transfer is related to propagation of electromagnetic waves in dielectric media, transmission lines and waveguides, where the dielectric permittivity determines the velocity of wave propagation, attenuation and ultimately the dimensions of the devices.

The most relevant physical processes in dielectric materials from the practical viewpoint are those which result in power loss. It is important to understand the basic characteristics of these processes because they determine the optimal approach to measurement.

Interaction of electromagnetic radiation with materials at frequencies of about 10^{12} Hz and above gives rise to quantized transitions between the electronic, vibrational and rotational molecular energy states, which can be observed by using appropriate quantum spectroscopy techniques. By contrast, the dielectric properties are governed by reorientational motions of molecular dipoles (dipolar relaxation) and motions of electrical charge carriers (electrical conduction), which leads to continuous dielectric dispersion and absorption that is observed in the frequency range of 10^{-6} Hz to 10^{12} Hz.

The dielectric relaxation [9.65] describes the dispersion of real permittivity ε' and the occurrence of dielectric absorption ε''. Permittivity measurements allows for the determination of molecular dipole moments and, subsequently, can link the relaxation process with molecular dynamics and structure. The dielectric absorption (loss) spectra as a function frequency and temperature [9.66, 67], can be used to characterize molecular dynamics in dipolar liquids (polar solvents and solutes), rotator-phase crystals, nonpolar and polar polymers (polyethylene, polyacrylates, epoxy resins, polyimides). Research on dielectric relaxation in molecular liquids and solids was pioneered by *Fröhlich* [9.68], *Hill* et al. [9.69], *Bottcher* and *Bordewijk* [9.70], and for macromolecules by *McCrum* et al. [9.71], and *Runt* and *Fitzgerald* [9.72]. Selected developments in dielectric and related molecular processs were reviewed by *Davies* [9.73]. Since 1954, the most widely known and comprehensive work on dielectric materials and corresponding measurements has been that of *von Hippel* [9.74]. Measurement of RF properties of materials were surveyed by *Bussey* [9.75]. Broadband waveguiding and free-space measurement methodologies for the agriculture industry were developed by *Nelson* and co-workers [9.76, 77]. Extensive dielectric data were obtained recently for ferroelectric ceramics (barium

titanate), inorganic and organic semiconductors and photoconductors, for ultra thin dielectrics films, which have important applications in solid-state electronic circuits and devices. Recent advances in the theory of dielectric relaxation and the corresponding experimental methodologies were reviewed by *Kremer* and *Schönhals* [9.78].

9.5.1 Dielectric Permittivity

The interaction of electromagnetic fields with matter is described by Maxwell's equations [9.79]. The polarization $\boldsymbol{P}$ describes the dielectric displacement $\boldsymbol{D}$ which originates from the response of the material to an external electric field $\boldsymbol{E}$

$$\boldsymbol{P} = \boldsymbol{D} - \varepsilon_0 \boldsymbol{E} = \left(\varepsilon_r^* \varepsilon_0 - \varepsilon_0\right) \boldsymbol{E} , \tag{9.68}$$

where ε_0 is the dielectric permittivity of free space ($\varepsilon_0 = 8.854 \times 10^{-12}$ F/m), and $\varepsilon^* = \varepsilon_0 \varepsilon_r^* = \varepsilon' - \mathrm{i}\varepsilon''$ is the complex permittivity tensor, which depends on temperature, frequency, and in the case of anisotropic materials, on the direction of the electric field vector $\boldsymbol{E}$. The frequency dependence of the permittivity is illustrated in Fig. 9.58.

Relative permittivity, ε_r^*, is a dimensionless ratio of complex permittivity to the permittivity of free space,

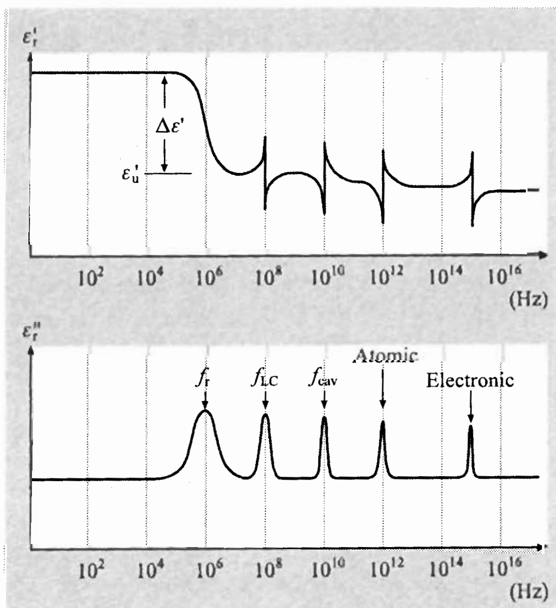

Fig. 9.58 Frequency dependence of the real ε_r', and imaginary ε_r'' parts of the complex permittivity with a single relaxation process at the relaxation frequency f_r

$\varepsilon_r^* = \varepsilon^*/\varepsilon_0 = \varepsilon_r' - \mathrm{i}\varepsilon_r''$. The dielectric constant is the real part of the relative permittivity. The symbol used in this document is ε_r' (Other symbols such as K, k, K', k', ε_r and ε' are symbols used in the technical literature.). Dielectric loss tangent $\tan(\delta)$ is a dimensionless ratio of the dielectric loss to the dielectric constant, $\tan(\delta) = \varepsilon_r''/\varepsilon_r'$. The real part of dielectric permittivity decreases by $\Delta\varepsilon_r'$ at a certain frequency f_r which gives rise to a corresponding peak of the dielectric loss ε_r''. Such frequency dependence of the complex permittivity indicates a *dielectric relaxation*. A dielectric material may exhibit several dielectric relaxation processes, each associated with its characteristic $\Delta\varepsilon_r'$, ε_r'' and f_r depending on the molecular mechanism involved.

The dielectric relaxation should not be confused with resonant transitions between vibrational and electronic states and those that originate from a resonant behavior of the electrical measurement circuit.

Dielectric Relaxation

Unlike *electrical conduction* in which charge carriers (electrons, ions and holes) move physically through the material under the influence of an electric field, the *dielectric relaxation* originates from reorientational responses of electric dipoles to the applied electric field. Materials in which the dipoles are induced only by the application of an electric field are nonpolar materials. Polar materials, on the other hand, have permanent molecular dipoles which may exhibit a number of different relaxation processes, each having a characteristic strength measured by $\Delta\varepsilon_r'$, and a characteristic relaxation frequency f_r. In the simplest case with a single relaxation time τ_r the dielectric relaxation function may be described by Debye's model [9.65], shown by (9.69). Here ε_u' is the dielectric constant at high frequencies, which does not contain a permanent dipole contribution ($\varepsilon_r' = \varepsilon_u'$ when $f \gg f_r$, Fig. 9.58).

$$\varepsilon^*/\varepsilon_0 = \varepsilon_u' + \frac{\Delta\varepsilon_r}{1 + \mathrm{i}\omega\tau_r} . \tag{9.69}$$

Cooperative distortional polarization, local rotational polarization and interfacial polarization are the most commonly observed relaxation processes. In a composite material, many or all of these processes may be present and give rise to a very complex relaxation behavior, which can be modeled as a superposition of several relaxations. The Havriliak–Negami (HN) relaxation function, defined below, has often been found to provide a good phenomenological description of dielectric relaxation data in molecular liquids, solids and glass

formers [9.80, 81]

$$\varepsilon^*/\varepsilon_0 = \sum_k \left(\varepsilon'_u + \frac{\Delta\varepsilon_r}{[1+(i\omega\tau_r)^\alpha]^\gamma} \right) , \quad k = 1, 2, 3 \dots . \tag{9.70}$$

The parameters α and γ describe the extent of symmetric (α) and asymmetric (γ) broadening of the complex dielectric function, where α and γ are ($0 < \alpha \leq 1$ and $0 < \alpha\gamma \leq 1$). Equation (9.70) reduces to the well-known Debye expression when $\alpha = \gamma = 1$. While the HN equation is often referred to as an 'empirical' relaxation function, recent modeling has linked the parameters α and γ to the degree of intermittency in molecular movement and long-lived spatial fluctuations in local material properties ('dynamic heterogeneity') [9.82], which gives some insight into the meaning of the fitted parameters. In this view, the exponent α is related to the temporal intermittency of molecular displacements while γ corresponds to long-lived 'dynamic heterogeneities' (or dynamic clusters). It is beyond the scope of this chapter to explain the theory of these processes and the reader is advised to consult references [9.83–86].

Regardless of the particular molecular mechanism of the dielectric relaxation, the phenomenological dependence of ε^*_r on frequency, as shown in Fig. 9.58, can be used as a guide to select an appropriate measurement method, and then be applied to describe and analyze the dielectric properties of most dielectric materials.

According to Fig. 9.58, the frequency spectrum can be divided into several regions, each corresponding to a characteristic dielectric response.

1. At low frequencies, well below f_r, dipoles easily respond and align with the applied alternating E-field without a time lag. The dielectric loss is negligibly small and the polarization as measured by ε'_r can achieve the maximum value, which depends on the statistical distribution of thermally induced molecular orientations and the amplitude of the applied field. At higher fields, polarization saturation may occur, where all the dipoles are aligned. The E-field induced polarization dominates over the thermal effects, giving rise to a *nonlinear dielectric response*.
2. At frequencies close to f_r, the molecular dipoles are too slow to reorient in phase with the alternating electric field. They lag behind and their contribution to ε'_r is smaller than that at low frequencies. This time lag or phase difference between $\boldsymbol{E}$ and $\boldsymbol{P}$ gives rise to the dielectric loss which peaks at f_r.
3. At frequencies above f_r the particular molecular dipoles cannot follow the electric field and do not contribute to ε'_r and ε''_r, and $\varepsilon'_r = \varepsilon'_u$.

It is important to note that the relaxation process always leads to a decrease of ε'_r with increasing frequency. Dipolar relaxation can be adequately described by an electrical equivalent circuit consisting of a capacitance C_s connected in parallel with resistance R_s which is illustrated in Fig. 9.59. Both, C_s and R_s can be experimentally measured and related to the material's dielectric properties ε'_r and ε''_r.

Resonant Transitions

The rapid oscillations of ε'_r shown in Fig. 9.58 at frequencies above f_r indicate a resonance. Similarly to relaxation, the resonance transitions are associated with the dielectric loss peak. However, the distinguished feature of a resonance transition is a singular behavior of ε'_r at the resonant frequency. From the dielectric metrology viewpoint, the most important resonances are the series resonance and the cavity resonance. These transitions are typically observed in the radio-frequency range and at microwave frequencies, respectively.

Series Inductance–Capacitance Circuit Resonance

Every electrical circuit consists of interconnecting leads that introduce finite residual inductance L_R. Therefore, when measuring a capacitance C_s there will be a certain frequency $f_{LC} = 1/(2\pi\sqrt{L_R C_s})$ at which a series resonance occurs. The equivalent electrical circuit for the series resonance consists of C_s in series with L_R. The residual resistance R_R is due to finite conductivity of the interconnects (Fig. 9.59). Since at f_{LC} the energy is concentrated in the magnetic field (or current) of the inductive component L_R rather than in the electric field in C_s, these resonance conditions generally are not use-

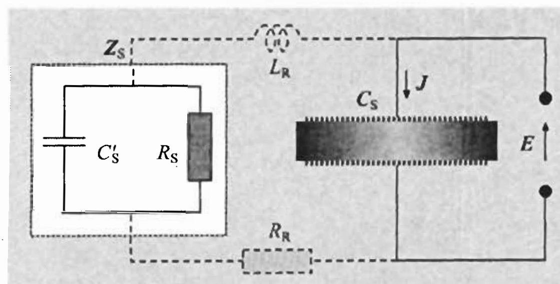

Fig. 9.59 Equivalent electrical circuit of a dielectric material

ful in measurement of the dielectric permittivity. The phenomenon is a common source of systematic errors in dielectric metrology unless the inductance is known or introduced purposely [9.87] to determine the capacitance from the resonant frequency. The characteristic feature of the series resonance is a rapid decrease in the measured complex impedance which reaches the value of R_R when the frequency approaches f_{LC}. The drop in the impedance is associated with an abrupt change of phase angle from $-\varphi$ to φ. The C_s value appears very large near f_{LC} when L_R is neglected in the equivalent circuit (Fig. 9.59), and consequently, it can be incorrectly interpreted as an apparent increase in the dielectric constant (Fig. 9.58).

Dielectric Resonance

When the dimensions (l) of the dielectric specimen are comparable with the guided wavelength $\lambda_g = \lambda_0/\sqrt{\varepsilon_r'}$ a superposition of the transmitted and reflected waves leads to a standing wave called cavity or dielectric resonance. At the resonant frequency, the electromagnetic energy is concentrated in the electric field inside the dielectric. Therefore the measurement techniques that are based on the dielectric resonators are the most accurate methods for determining the dielectric permittivity of low loss materials.

Infrared and Optical Transitions

Interaction of electromagnetic radiation with materials at frequencies of about 10^{12} Hz and above gives rise to quantized resonant transitions between the electronic, vibrational and rotational molecular energy states. These transitions are responsible for a singular behavior of the dielectric permitivity and the corresponding absorption, which can be observed by using appropriate quantum spectroscopy techniques. These quantum spectroscopies form a large part of modern chemistry and physics. At optical frequencies the materials dielectric properties are described by complex optical indices, $n^* = \sqrt{\varepsilon^*}$, rather than permittivity.

9.5.2 Measurement of Permittivity

Techniques for complex permittivity measurement may be subdivided into two general categories [9.74]:

1. The frequency range over which the dielectric specimen maybe treated as lumped parameter components;
2. The high frequency range where the wavelength of the electric field is comparable to the physical dimensions of the dielectric specimen and, as a consequence, it is often referred as a distributed parameter system.

Dielectric Measurements Using Lumped Parameter Specimens

In the low frequency range, where the wave propagation effects can be neglected, the equivalent complex impedance $\boldsymbol{Z}_s$ of the relaxation circuit shown in Fig. 9.59 can be measured to determine the capacitance $\boldsymbol{C}_s$ and then the material's relative complex permittivity ε_r^*.

When a capacitor is filled with a dielectric material (Sect. 9.1.6) the resulting capacitance is $\boldsymbol{C}_s$ and the dielectric permittivity is defined by (9.71)

$$\varepsilon_r^*(\omega) = \varepsilon_r'(\omega) - i\varepsilon_r''(\omega) = \boldsymbol{C}_s(\omega)/C_0 \,, \quad (9.71)$$

where C_0 is the capacitance of the empty cell and ω is the angular frequency ($\omega = 2\pi f$).

If the sinusoidal electric field $\boldsymbol{E}(\omega) = E_0 \exp(i\omega t)$ is applied to $\boldsymbol{C}_s$ then the dielectric permittivity can be determined by measuring the complex impedance Z_s of the circuit.

$$\frac{1}{\boldsymbol{Z}_s(\omega)} = i\omega \boldsymbol{C}_s \,, \quad (9.72)$$

$$\varepsilon^*(\omega) = \frac{1}{i\omega \boldsymbol{Z}_s(\omega) C_0} \,, \quad (9.73)$$

where $\boldsymbol{J}(\omega)$ is the complex current density. Consistent with the electrical equivalent circuit consisting of the real capacitance C_s' in parallel with a resistance R_s the impedance is given by

$$\frac{1}{\boldsymbol{Z}_s(\omega)} = \frac{1}{R_s} + i\omega C_s' \quad (9.74)$$

and the direct expressions for ε_r' and ε_r'' are

$$\varepsilon_r' = \frac{C_s'}{C_0} \,, \quad (9.75)$$

$$\varepsilon_r'' = \frac{1}{\omega R_s C_0} \,. \quad (9.76)$$

The capacitance of the empty cell C_0 (cell constant) is typically determined from the specimen geometry or measurements of standard materials with known dielectric permittivity. Commercially available dielectric test fixtures have the cell constant and error correction formulas provided by their manufacturers [9.88, 89].

Impedance Measurement Using a Four-Terminal Method

In the frequency range of up to about 10^8 Hz, a four terminal (4T) impedance analyzer can be employed to

measure complex impedance of the capacitance C_s and then the permittivity can be calculated from expressions (9.74–9.76). The 4T methodology refers to the direct phase sensitive measurement of the sample's current and voltage. Systems combining Fourier correlation analysis with dielectric converters and impedance analysis have recently become commercially available [9.78]. The recently developed dielectric instrumentation incorporates into one device a digital synthesizer-generator, sine wave correlators and phase sensitive detectors, capable of automatic impedance measurements from 10^{-2} to $10^{13}\,\Omega$. The broad impedance range also allows a wide capacitance measurement range with resolution approaching 10^{-15} F. The instrumentation should be calibrated against appropriate impedance standards using methods and procedures recommended by their manufacturers.

The dielectric samples typically utilize a parallel-plate or cylindrical capacitor geometry [9.74,90] having capacitances of about 10 pF to several hundred pF. The standard measurement procedures [9.90] recommend a three-terminal (3T) cell configuration with a guard electrode (G), which minimizes the effect of the fringing and stray electric fields on the measurements. The optimal method for connecting a 3T cell to a 4T impedance analyzer is shown in Fig. 9.60.

The "High" current on voltage terminals should be connected via coaxial cables directly to the un-guarded electrode 'H', while the "Low" current and voltage should be connected to the electrode that is surrounded by the guard electrode. Note that the return current loop of coaxial shields connections 'S' should be short and connected to 'G' at a single common point. The return current loop is absolutely necessary for accurate impedance measurements, especially above 1 MHz. In a two terminal configuration (2T) without the guard electrode, the connections 'S' should be simply grounded together.

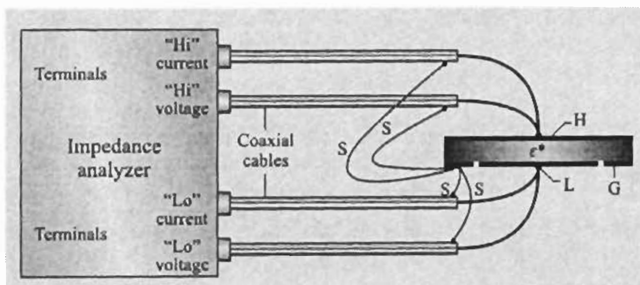

Fig. 9.60 a 3T cell to an 4T impedance analyzer. (H) and (L) are the high and low potential electrodes respectively; 'G' is the guard electrode; (S) are the return current loops of coaxial shield connections

The dielectric constant, dielectric loss and the relaxation frequency are temperature dependent. Therefore, it is essential to measure the specimen temperature and to keep it constant (isothermal conditions) during the measurements.

Impedance Measurements Using Coaxial Line Reflectometry

In the 4T configuration the residual inductance L_R of interconnecting cables contributes to the circuit impedance creating conditions for the series resonance at $f_{LC} \approx 1/(2\pi\sqrt{L_R C_s'})$, which limits the usable frequency range. Typically, the series resonance occurs above about 30 MHz. Impedance at higher frequencies may be determined from the reflection coefficient using microwave techniques with precision transmission lines. In these techniques the reference plane can be setup right at the specimen section which largely eliminates propagation delay due to L_R. When a dielectric specimen of impedance $\boldsymbol{Z}_s$ terminates a transmission line that has a known characteristic impedance Z_0 and known wave propagation characteristic, the impedance mismatch between the line and the specimen results in reflection of the incoming wave. The relation between $\boldsymbol{Z}_s$ and complex reflection coefficient $\boldsymbol{\Gamma}$ is given by (9.77) [9.91,92]

$$\boldsymbol{\Gamma} = \frac{\boldsymbol{Z}_s - Z_0}{\boldsymbol{Z}_s + Z_0}\,. \tag{9.77}$$

It follows from (9.77) that when the line is terminated with a *short* ($\boldsymbol{Z}_{short} = 0$) then $\boldsymbol{\Gamma} = -1$. For an *open* termination ($\boldsymbol{Z}_{open} = \infty$) $\boldsymbol{\Gamma} = 1$, while in the case of a matched load, when $\boldsymbol{Z}_s = Z_0$, $\boldsymbol{\Gamma} = 0$, which results in no reflection. These three terminations, i. e. *short, load and open*, are used as calibration standards for setting-up the reference plane and proper measurement conditions of the reflection coefficient at the specimen section.

Many coaxial line configurations are available in the RF and microwave ranges, each designed for a specific purpose and application. The frequency range is limited by the excitation of the first circular waveguide propagation mode in the coaxial structure [9.91]. Decreasing the diameter of the outer and inner conductors increases the highest usable frequency. The following is a brief review of coaxial line configurations, having Z_0 of 50 Ω, most commonly used for microwave testing and measurements [9.93].

Precision APC-7 mm Configuration

The APC-7 (Amphenol Precision Connector-7 mm) utilizes air as a dielectric medium between the inner and outer conductors. It offers the lowest reflection coefficient and most repeatable measurement from DC to 18 GHz, and is the preferred configuration for the most demanding applications, notably metrology and calibration. The diameter of the inner conductor $d = 3.02$ mm and the diameter of the outer conductor $D = 7.00$ mm (Fig. 9.61) determines the characteristic impedance value of 50 Ω [9.91].

Precision APC-3.5 mm Configuration

The 3.5 mm configuration also utilizes air as a dielectric medium between the inner and outer conductors. It is mode free up to 34 GHz.

Precision-2.4 mm Configuration

The 2.4 mm coaxial configuration was developed by Hewlett Packard and Amphenol for use up to 50 GHz. It can mate with the APC 3.5 mm connector through appropriate adapters. The 2.4 mm coaxial line is offered in three quality grades: general purpose, instrument, and metrology. The general purpose grade is intended for economy use on components and cables. Instrument grade is best suited for measurement applications where repeatability and long life are primary considerations. Metrology grade is best suited for calibration applications where the highest performance and repeatability are required.

1.85 mm Coaxial Configuration

The 1.85 mm configuration was developed in the mid-1980s by Hewlett Packard, now Agilent Technologies, for mode-free performance to about 65 GHz. HP offered their design to the public domain in 1988 to encourage standardization of this connector types. Nevertheless, few devices and instrumentation are available today from various manufacturers, mostly for research work. The 1.85 mm connector mates with the 2.4 mm connector.

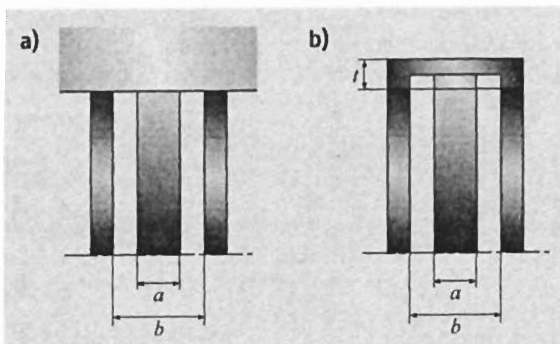

Fig. 9.61 (a) Open-ended, (b) and short terminated coaxial test fixture

1.0 mm Coaxial Configuration

Designed to support transmission all the way up to 110 GHz, approaching optical frequencies. This 1.0 mm coaxial configuration, including the matching adapters and connectors, is a significant achievement in precision microwave component manufacturing.

There is a large family of coaxial test fixtures designed for dielectric measurements. *Open-ended coaxial test fixtures* (Fig. 9.61a) are widely used for characterizing thick solid materials and liquids [9.94], and are commercially available (Agilent, Novocontrol Dielectric Probes) [9.95]. The measurements are conveniently performed by contacting one flat surface of the specimen or by immersing the probe in the liquid sample.

Short-terminated probes (Fig. 9.61b) are better suited for thin film specimens. Dielectric materials of precisely known permittivity (air, water) are often used as a reference for correcting systematic errors in measuring $\boldsymbol{\Gamma}$ that are due to differences between the measurement and the calibration configurations. If the relaxation circuit satisfies the lumped parameters, then ε'_r and ε''_r can be obtained by combining (9.73) and (9.77) [9.96]:

$$\varepsilon'_r = \frac{-2\,|\boldsymbol{\Gamma}|\sin\phi}{\omega Z_0 C_0\left(1 + 2\Gamma\cos\phi + |\boldsymbol{\Gamma}|^2\right)}\,, \tag{9.78}$$

$$\tan\delta = \frac{\varepsilon''_r}{\varepsilon'_r} = \frac{1 - |\boldsymbol{\Gamma}|^2}{-2\,|\boldsymbol{\Gamma}|\sin\phi}\,. \tag{9.79}$$

In practice, the conventional lumped parameter formulas (9.78, 9.79) and the corresponding test procedures are accurate up to a frequency at which the impedance of the specimen decreases to about one tenth (0.1) of the characteristic impedance of the coaxial line. Since the standard characteristic impedance of coaxial configuration listed above is 50 Ω, the lowest usable impedance value of lumped-parameter circuits is about 5 Ω, hence, $f_{max} \approx 1/(10\pi C'_s)$ [9.97]. Depending on the specimen permittivity and thickness, this upper frequency limit in the APC-7 configuration is typically below 5 GHz. At frequencies $f > f_{max}$, wave propagation causes a spatial distribution of the electric field inside the specimen section which can no longer be treated as a lumped capacitance and has to be analyzed as a microwave network.

Dielectric Measurements Using Microwave Network Analysis

Microwave network analyzer terminology describes measurements of the incident, reflected, and transmitted electromagnetic waves. The reflected wave is measured at the Port 1, and the transmitted wave is measured at Port 2 (Fig. 9.62).

If the amplitude and phase of these waves are known, then it is possible to quantify the reflection and transmission characteristics of a material under test (MUT) with its dielectric permittivity and the dimensions of the test fixture. The reflection and transmission parameters can be expressed as vector (magnitude and phase), scalar (magnitude only), or phase-only quantities. In this notation, impedance and reflection coefficient are vectors. Network characterization at low frequencies is usually based on measurement of complex voltage and current at the input or output ports (terminals) of a device. Since it is difficult to measure total current or voltage at high frequencies, complex scattering parameters, S_{11}, S_{12}, S_{21} and S_{22} are generally measured instead [9.98, 99]. Measurements relative to the incident wave allow to normalize and quantify the reflection and transmission measurements to obtain values that are independent of both, absolute power and variations in source power versus frequency. The scattering parameters (S-parameters) are defined by (9.80) [9.99]

$$\begin{aligned} b_1 &= S_{11}a_1 + S_{12}a_2 , \\ b_2 &= S_{21}a_1 + S_{22}a_2 . \end{aligned} \tag{9.80}$$

A general signal flow graph of a two-port network with the corresponding scattering parameters is shown in Fig. 9.63a. Here a_1 and a_2 are the complex amplitudes of the waves entering the network, while b_1 and b_2 are complex amplitudes of the outgoing waves. Figure 9.63b shows a termination or load having reflection coefficient $\boldsymbol{\Gamma}$. Since there is no transmitted wave to Port 2, $b_2 = 0$, $\boldsymbol{\Gamma} = b_1/a_1 = S_{11}$.

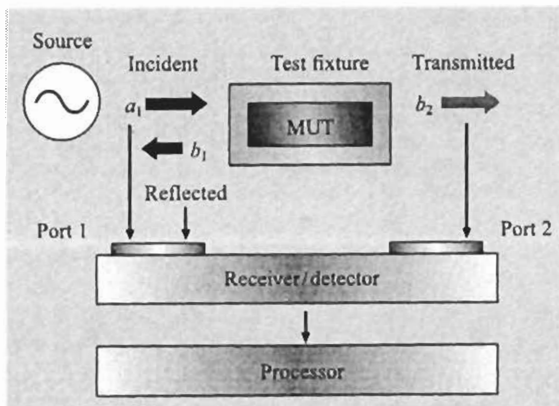

Fig. 9.62 Block diagram of a network analyzer

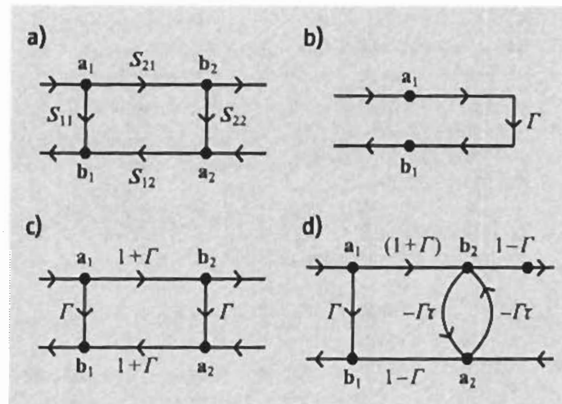

Fig. 9.63a–d Scattering parameters signal flow diagrams: **(a)** two-port network, **(b)** load termination, **(c)** shunt admittance, **(d)** transmission line partially filled with a dielectric slab

The number of S-parameters for a given device is equal to the square of the number of ports. For example, a two-Port device has four S-parameters. The numbering convention for S-parameters is that the first number following the S is the Port at which energy emerges, and the second number is the port at which energy enters. So S_{21} is a measure of power emerging from port 2 as a result of applying an RF stimulus to Port 1. When the numbers are the same (e.g. S_{11}, S_{22}), it indicate a reflection measurement. The measured S-parameters of multiple devices can be cascaded to predict performance of more complex networks. Figure 9.63c is a shunt discontinuity, such as the junction of two lines or impedance mismatch where $S_{11} = S_{22} = \boldsymbol{\Gamma}$, while $S_{12} = S_{21} = 1 + \boldsymbol{\Gamma}$. Figure 9.63d shows the flow diagram for a transmission line, which is partially filled with a dielectric material of finite length l [9.100]. This network has a practical application in the dielectric measurements using the reflection-transmission method described in the next chapter.

Two-Port Transmission–Reflection Method

A dielectric specimen partially filling a coaxial air-line (Fig. 9.64) causes impedance mismatch and multiple wave reflections, which can be modeled as a two port network.

The scattering parameters S_{11} and S_{21} at the reference planes A and B for a specimen having the dielectric

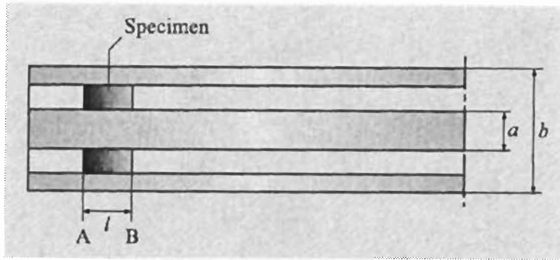

Fig. 9.64 Test fixture for dielectric measurement using the reflection-transmission method

permittivy ε_r^* can be obtained from the flow graph shown in Fig. 9.63d [9.100, 101]

$$S_{11}(\omega) = \frac{(1-\tau^2)\Gamma}{1-\tau^2\Gamma^2}\,, \tag{9.81}$$

$$S_{21}(\omega) = \frac{(1-\Gamma^2)\tau}{1-\tau^2\Gamma^2}\,, \tag{9.82}$$

$$\Gamma = \frac{Z_s - Z_0}{Z_s + Z_0} = \frac{1-\sqrt{\varepsilon_r^*}}{1+\sqrt{\varepsilon_r^*}}\,, \tag{9.83}$$

where Γ is the complex reflection coefficient for non-magnetic media, τ is the transmission coefficient

$$\tau = \mathrm{e}^{-\mathrm{i}\gamma l} \tag{9.84}$$

and γ is the propagation constant, $\gamma = \mathrm{i}\omega/c\sqrt{\varepsilon_r^*}$.

Using an APC-7 beadless coaxial air line as a sample holder with $d = 3.02$ mm and $D = 7.0$ mm, the dielectric permittivity can be measured up to 18 GHz [9.102].

The dielectric specimen for the transmission-reflection method described above must be machined precisely to fit dimensions of the inner (a) and outer (b) conductors of the coaxial line [9.103].

One-Port Reflection Method

Another important application of network analysis to the high frequency dielectric metrology is the measurement of dielectric permittivity of thin films in a short-terminated coaxial test fixture (Fig. 9.61b).

The scattering parameter of the test specimen treated as a transmission line with capacitance is given by (9.85), while the corresponding expression for impedance is given by (9.86) [9.104, 105]

$$S_{11}(\omega) = \frac{\Gamma + \tau}{1 + \Gamma\tau}\,, \tag{9.85}$$

$$Z_s = \frac{x\cot(x)}{\mathrm{i}\omega C_s} + \mathrm{i}\omega L_s\,, \tag{9.86}$$

where x is the wave propagation parameter

$$x = \omega l\sqrt{\varepsilon_r^*}/2c\,, \tag{9.87}$$

$$L_s = 1.27\times 10^{-7}\,(\mathrm{H/m})\times d\,(\mathrm{m}) \tag{9.88}$$

$$\varepsilon_r^* = \frac{x\cot(x)}{\mathrm{i}\omega C_0\left[Z_0(1+S_{11})/(1-S_{11}) - \mathrm{i}\omega L_s\right]}\,. \tag{9.89}$$

Equations (9.87) and (9.88) have been validated numerically and experimentally up to the first cavity resonance

$$f_{\mathrm{cav}} = \frac{c}{l\,\mathrm{Re}\left(\sqrt{\varepsilon_r^*}\right)} \approx 121/\left[\sqrt{\varepsilon_r}\,(\mathrm{GHz})\right]\,, \tag{9.90}$$

where Re indicates the real part of the square root of complex permittivity and $l = 2.47$ mm, which is the propagation length for the APC-7 test fixture presented in Fig. 9.61b [9.105]. For example, in the case where a specimen has a dielectric constant of 100, f_{cav} is about 12 GHz.

Resonant Cavity Methods

Resonant measurement methods are the most accurate in determining the dielectric permittivity. In order to excite a resonance the materials must have a low dielectric loss ($\varepsilon_r'' < 10^{-3}$). The measurements are usually limited to the microwave frequency range. A fairly simple and commonly used resonant method for measurement of microwave permittivity is the resonant cavity perturbation method [9.106]. Figure 9.65 illustrates a cavity test fixture which is a short section of rectangular waveguide. Conducting plates bolted or soldered to the end flanges convert the waveguide into a resonant box. A small iris hole in each end plate feeds microwave energy into and out of the cavity. Clearance holes centered in opposite walls are provided for a dielectric specimen, which

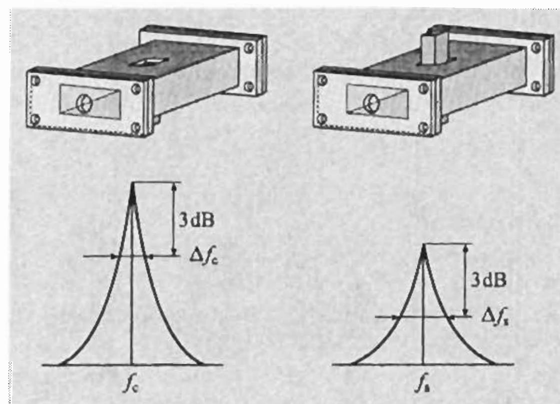

Fig. 9.65a,b Scattering parameter $|S_{21}|$ measured for **(a)** an empty test fixture and **(b)** for test fixture with a specimen inserted

is placed into region of maximum electric field. The measurement frequency is limited to few values corresponding to the fundamental mode and few higher order modes. Typically standard rectangular waveguide for the X-band [9.102] is used as a test fixture that covers the frequency range from 8 GHz to 12 GHz. The test specimen may have the shape of a cylindrical rod, sphere or a rectangular bar [9.106].

The test fixture is connected to a network analyzer (Fig. 9.62) by using appropriate adapters and cables. The resonance is indicated by a sharp increase in the magnitude of the $|S_{21}|$ parameter, with a peak value at the resonant frequency. When the dielectric specimen is inserted to the empty (air filled) cavity the resonant frequency decreases from f_c to f_s while the bandwidth Δf at half power, i. e. 3 dB below the $|S_{21}|$ peak, increases from Δf_c to Δf_s (see illustration in Fig. 9.65). A shift in resonant frequency is related to the specimen dielectric constant, while the larger bandwidth corresponds to a smaller quality factor Q, due to dielectric loss. The cavity perturbation method involves measurement of f_c, Δf_c, f_s, Δf_s, and volume of the empty cavity V_c and the specimen volume V_s.

The quality factor for the empty cavity and for the cavity filled with the specimen is given by expression (9.91)

$$Q_c = f_c/\Delta f_c\,, \quad Q_s = f_s/\Delta f_s\,. \tag{9.91}$$

The real and imaginary parts of the dielectric constant are given by (9.92) and (9.93), respectively

$$\varepsilon_r' = \frac{V_c(f_c - f_s)}{2V_s f_s}\,, \tag{9.92}$$

$$\varepsilon_r'' = \frac{V_c}{4V_s}\left(\frac{1}{Q_s} - \frac{1}{Q_c}\right)\,. \tag{9.93}$$

The resonant cavity perturbation method described above requires that the specimen volume be small compared to the volume of the whole cavity ($V_s < 0.1 V_c$), which can lead to decreasing accuracy. Also, the specimen must be positioned symmetrically in the region of maximum electric field. However, compared to other resonant test methods, the resonant cavity perturbation method has several advantages such as overall good accuracy, simple calculations and test specimens that are easy to shape. Moreover, circular rods, rectangular bars or spheres are the basic designs that have been widely used in manufacturing ceramics, ferrites and organic insulting materials for application in the microwave communication and electric power distribution.

There is a large number of other resonant techniques described in the technical and standard literature, each having a niche in the specific frequency band, field behavior and loss characteristic of materials. Some of these are briefly described below:

Sheet low loss materials can be measured at X-band frequencies by using a split cavity resonator [9.107]. The material is placed between the two sections of the splitable resonator. When the resonant mode is excited the electric field is oriented parallel to the sample plane.

The split-post dielectric resonator technique [9.108] is also suitable for sheet materials. The system is excited in the transfer electromagnetic azimuthal mode. A useful feature of this type of resonant cavity is the ability to operate at lower frequencies without the necessity of using use large specimens.

Parallel-plate resonators [9.109] with conducting surfaces allow measurements at lower frequencies since the guided wavelength λ_g inside the dielectric is smaller than in the air-filled cavities by a factor of approximately $\sqrt{\varepsilon_r'}$. The full-sheet resonance technique [9.110] is commonly used to determine the permittivity of copper clad laminates for printed circuit boards.

9.5.3 Uncertainty Considerations

With increasing frequency, the complexity of the dielectric measurement increases considerably. Several uncertainty factors such as instrumentation, dimensional uncertainty of the test specimen geometry, roughness and conductivity of the conduction surfaces contribute to the combined uncertainty of the measurements. The complexity of modeling these factors is considerably higher within the frequency range of the LC resonance. Adequate analysis can be performed, however, by using the partial derivative technique [9.111] and considering the instrumentation and the dimensional errors. Typically, the standard uncertainty of S_{11} can be assumed to be within the manufacturer's specification for the network analyzer, about ± 0.005 dB for the magnitude and $\pm 0.5°$ for the phase. The combined relative standard uncertainty in geometrical capacitance measurements is typically smaller than 5%, where the largest contributing factor is the uncertainty in the film thickness measurements. Equation (9.88), for example, allows evaluation of systematic uncertainty due to residual inductance. It has been validated empirically for specimens 8 μm to 300 μm thick for measurements in the frequency range of 100 MHz to 12 GHz. These are reproducible with relative combined uncertainty in ε_r' and ε_r'' of better than 8% for specimens having $\varepsilon_r' < 80$ and thickness $d < 300$ μm. The resolution in the dielectric loss tangent measurements is < 0.005. Additional limitations may

arise from the systematic uncertainty of the particular instrumentation, calibration standards and the dimensional imperfections of the implemented test fixture. Furthermore, the results of impedance measurements may not be reliable at frequencies, where $|Z|$ decreases below 0.05 Ω.

9.5.4 Conclusion

In summary, one technique alone is typically not sufficient to characterize dielectric materials over the entire frequency and temperature range of interest. The broadband one-port reflection method (9.86–9.89) is most suitable for thin high dielectic constant films that are of interest to electronics, bio- and nano-technologies. For bulk anisotropic dielectics, the two-port transmission reflection method (9.81–9.84) is best. These materials must be machined to a toroidal shape to precisely fit the test coaxial test fixture. The resonant cavity method (9.91–9.93) is best for evaluating low-loss solid dielectric materials having the standard shapes used in manufacturing ceramics, ferrites, and organic insulting materials for application in microwave communication and electric power distribution. It is very important to use proper method for a given situation. Therefore measurements of dielectric substrates, films, circuit board materials, ceramics or ferrites always present a metrological challenge.

References

9.1 R. E. Hummel: *Understanding Materials Science*, Chap. 11, Electrical Properties of Materials (Springer, New York, Berlin 2004) pp. 185–222

9.2 C. H. He, Z. Lu, S. Liu, R. Liu: Cross-conductivity standard for non-ferrous metals, IEEE Trans. IM **44**, 181–183 (1995)

9.3 G. Rietveld, C. V. Koijmans, L. C. A. Henderson, M. J. Hall, S. Harmon, P. Warnecke, B. Schumacher: DC conductivity measurements in the van der Pauw geometry, IEEE Trans. IM **52**, 449–453 (2003)

9.4 L. J. van der Pauw: A method of measuring specific resistivity and Hall effect of discs of arbitrary shape, Philips Res. Rep. **13**, 1–9 (1958)

9.5 DIN IEC 468: *Method of Measurement of Resistivity of Metallic Materials* (Beuth, Berlin 1981)

9.6 NPL Report DEM-ES 001: Techniques and materials for the measurement of DC and AC conductivity of non-ferrous metals and alloys, *Conductivity*, May 2004. The *Conductivity* project is (has been) financially supported by an EU grant (contract no. G6RD-CT-2000-00210) under the EU Growth programme, part of the 5th Framework programme

9.7 M. J. Hall, L. C. A. Henderson, G. Ashcroft, S. Harmon, P. Warnecke, B. Schumacher, G. Rietveld: Discrepancies between the DC and AC measurement of low frequency electrical conductivity, Dig. Conf. Proc. Electrom. Meas. CPEM 2004, London (2004) pp. 34–35

9.8 A. C. Lynch, A. E. Drake, C. H. Dix: Measurement of eddy-current conductivity, IEE Proc. Sci. Meas. Technol. **130**, 254–260 (1983)

9.9 H. Kamerlingh Onnes: The superconductivity of mercury, Leiden Commun. **122b**, 1240 (1911)

9.10 J. Bardeen, L. N. Cooper, J. R. Schrieffer: Theory of superconductivity, Phys. Rev. **108**, 1175–1204 (1957)

9.11 J. G. Bednorz, K. A. Müller: Possible high-T_c superconductivity in the Ba-La-Cu-O system, Z. Phys. B **64**, 189–193 (1986)

9.12 M. K. Wu, J. R. Ashburn, C. J. Torng, P. H. Hor, L. R. Meng, L. Gao, Z. J. Huang, Y. Q. Wang, C. W. Chu: Superconductivity in a new mixed phase Y-Ba-Cu-O system at ambient pressure, Phys. Rev. Lett. **58**, 908–910 (1987)

9.13 C. N. R. Rao, R. Nagarajan, R. Vijayaraghavan: Synthesis of cuprate superconductors, Supercond. Sci. Technol. **6**, 1–22 (1993)

9.14 J. Clarke, A. I. Braginski: *The SQUID Handbook, Fundamentals and Technology of SQUIDs and SQUID Systems*, Vol. 1 (Wiley, New York 2004)

9.15 B. D. Josephson: Possible new effects in superconductive tunneling, Phys. Lett. **1**, 251–253 (1962)

9.16 R. Pöpel: The Josephson effect and voltage standards, Metrologia **29**, 153–174 (1992)

9.17 S. A. Keys, D. P. Hampshire: *Characterization of the transport critical current density for conductor applications, Handbook of Superconducting Materials II: Characterization, Applications and Cryogenics*, ed. by D. A. Cardwell, D. S. Ginley (IOPP, London 2003) p. 1297

9.18 W. Meissner, R. Ochsenfeld: Ein neuer Effekt bei Eintritt der Supraleitfähigkeit, Naturwiss. **21**, 787 (1933) (in German)

9.19 DIN EN IEC 61788-1: *Superconductivity – Critical, Current Measurement – DC Critical Current of Cu/Nb-Ti Composite Superconductors* (Beuth, Berlin 1999)

9.20 P. W. Atkins: *Physikalische Chemie*, 3rd edn. (VCH, Weinheim 1990) pp. 3834–846 German transl.

9.21 C. H. Hamann, W. Vielsich: *Elektrochemie*, 3rd edn. (VCH, Weinheim 1998)

9.22 J. M. G. Barthel, H. Krienke, W. Kunz: *Physical Chemistry of Electrolyte Solutions – Modern Aspects; Top. Phys. Chem.*, Vol. 5, ed. by J. M. G. Barthel, H. Krienke, W. Kunz (Springer, Berlin, Heidelberg 1998)

9.23 J. O. M. Bockris, A. K. N. Reddy, K. N. Amlya: *Modern Electrochemistry 1, Ionics*, 2nd edn. (Springer, Berlin, Heidelberg 1989) p. 379

9.24 O. F. Mohammed, D. Pines, J. Dreyer, E. Pines, E. T. J. Nibbering: Sequential proton transfer through water bridges in acid-base reactions, Science **310**, 83–86 (2005)

9.25 F. Brinkmann, N. E. Dam, E. Deák, F. Durbiano, E. Ferrara, J. Fükö, H. D. Jensen, M. Máriássy, R. H. Shreiner, P. Spitzer, U. Sudmeier, M. Surdu: Primary methods for the measurement of electrolytic conductivity, Accred. Qual. Assur. **8**, 346–353 (2003)

9.26 United States Pharmacopeia: USP 27-NF 22 (U.S. Pharmacopoeia, Rockville 2004)

9.27 ISO 7888: 1985 Water Quality: Determination of electrical conductivity (ISO, Geneva 1985)

9.28 Y. C. Wu, K. W. Pratt, W. F. Koch: Determination of the absolute specific conductance of primary standard KCl solutions, J. Solution Chem. **18**, 515–528 (1989)

9.29 G. Jones, S. M. Christian: The measurement of the conductance of electrolytes. VI. Galvanic polarization by alternating current, J. Am. Chem. Soc. **57**, 272–284 (1935)

9.30 P. Spitzer, U. Sudmeier: *Electrolytic conductivity—A new subject field at PTB, Report on the 146 PTB Seminar Electrolytic Conductivity*, ed. by P. Spitzer, U. Sudmeier (PTB-ThEx-15, Physikalisch-Technische Bundesanstalt, Braunschweig 2000) pp. 39–47

9.31 P. Saulnier: Absolute determination of the conductivity of electrolytes. Double differential cell with adjustable constant, J. Solution Chem. **8**, 835–845 (1979)

9.32 P. Saulnier, J. Barthel: Determination of electrolytic conductivity of a 0.01 D aqueous potassium chloride solution at various temperatures by an absolute method, J. Solution Chem. **8**, 847–851 (1979)

9.33 F. Löffler: *Design and production of the electric conductivity cell, Report on the 146 PTB Seminar Electrolytic Conductivity*, ed. by P. Spitzer, U. Sudmeier (PTB-ThEx-15, Physikalisch Technische Bundesanstalt, Braunschweig 2000) pp. 49–64

9.34 Y. C. Wu, W. F. Koch, D. Feng, L. A. Holland, A. E. Juhász, A. Tomek: A DC method for the absolute dtermination of conductivities of the primary standard KCl solutions from 0 °C to 50 °C, J. Res. Natl. Inst. Stand. Technol. **99**, 241–224 (1994)

9.35 D. F. Evans: *The measurement and interpretation of electrolytic conductivity, Techn. Electrochem.* **2** (Wiley, New York 1973)

9.36 T. S. Light: Temperature dependence and measurement of resistivity of pure water, Anal. Chem. **56**, 1138–1142 (1994)

9.37 Radiometer Analytical: *Conductivity Theory and Practice*, Radiometer Analytical, Villeurbanne, France www.radiometer-analytical.com

9.38 European Pharmacopeia: *Conductivity*, EP 4, 2.2.38 (European Pharmacopeia, Strasbourg 2004) (http://www.pheur.org/)

9.39 W. L. Marshall: Electrical conductance of liquid and supercritical water evaluated from 0 °C and 0.1 MPa to high temperatures and pressures. Reduced-state relationships, J. Chem. Eng. Data **32**, 221–226 (1987)

9.40 R. D. Thornton, T. S. Light: A new approach to accurate resistivity measurement of high purity water, Ultrapure Water **7** (1989)

9.41 P. Spitzer, B. Rossi, Y. Gignet, S. Mabic, U. Sudmeier: New approach to calibrating conductivity meters in the low conductivity range, Accred. Qual. Assur. **10**, 78–81 (2005)

9.42 H. D. Jensen, J. Sørensen: *Electrolytic conductivity at DFM—results and experiences, Report on the 146 PTB Seminar Electrolytic Conductivity*, ed. by P. Spitzer, U. Sudmeier (PTB-ThEx-15, Physikalisch-Technische Bundesanstalt, Braunschweig 2000) pp. 153–13

9.43 D. C. Look: *Electrical Characterization of GaAs Materials and Devices* (Wiley, Chichester 1989)

9.44 P. Blood, J. W. Orton: *The Electrical Characterization of Semiconductors: Majority Carriers and Electron States* (Academic, New York 1992)

9.45 E. B. Hansen: On the influence of shape and variations in conductivity of the sample on four-point measurements, Appl. Sci. Res. B **8**, 93–104 (1960)

9.46 R. L. Petritz: Theory of an experiment for measuring the mobility and density of carriers in the space-charge region of a semiconductor surface, Phys. Rev. **110**, 1254–1262 (1958)

9.47 L. J. van der Pauw: A method of measuring specific resistivity and hall effect of discs of arbitrary shape, Philips Res. Rep. **13**, 1–9 (1958)

9.48 S. M. Sze: *Physics of Semiconductor Devices* (Wiley, Chichester 1981)

9.49 K. Ziegler, E. Klausmann, S. Kar: Determination of the semiconductor doping profile right up to its surface using the MIS capacitor, Solid-State Electron. **18**, 189–198 (1975)

9.50 D. P. Kennedy, P. C. Murley, W. Kleinfelder: On the measurement of impurity distributions in silicon by the differential capacitance technique, IBM J. Res. Dev, 399–409 (Sept. 1968)

9.51 D. P. Kennedy, R. P. O'Brian: On the measurement of impurity atom distributions by the differential capacitance technique, IBM J. Res. Dev. 212–214 (March 1969)

9.52 W. C. Johnson, P. T. Panousis: The influence of Debye length on the C–V-measurement of doping profiles, IEEE Trans. ED **18**, 956–973 (1971)

9.53 W. A. Harrison: *Electronic Structure and the Properties of Solids: The Physics of the Chemical Bond* (Dover, New York 1989)

9.54 S.R. Forest, R. F. Leheny, R. E. Nahory, M. A. Pollack: $In_{0.53}Ga_{0.47}As$ photodiodes with dark current limited by generation-recombination and tunneling, Appl. Phys. Lett. **37**(3), 322–325 (1980)

© Springer 2006

9.55 A. Goetzberger, B. McDonald, R. H. Haitz, R. M. Scarlett: Avalanche effects in silicon p-n junction. II. structurally perfect junctions, J. Appl. Phys. **34**, 1591 ff. (1963)

9.56 G. L. Miller, D. V. Lang, L. C. Kimerling: Capacitance transient spectroscopy, Ann. Rev. Mater. Sci. **7**, 377–448 (1977)

9.57 D. V. Lang: Deep-level transient spectroscopy, J. Appl. Phys. **45**(7), 3023–3032 (1974)

9.58 R. N. Hall: Electron-hole recombination in germanium, Phys. Rev. **87**, 387 (1952)

9.59 W. Shockley, W. T. Read: Statistics of the recombinations of holes and electrons, Phys. Rev. **87**, 835–842 (1952)

9.60 D. L. Partin, J. W. Chen, A. G. Milnes, L. F. Vassamillet: J. Appl. Phys. **50**(11), 6845 ff (1979)

9.61 E. H. Rhoderick: *Metal-Semiconductor Contacts* (Clarendon, Oxford 1980)

9.62 A. Piotrowska, A. Guivarc'h, G. Pelous: Ohmic contacts to III-V compound semiconductors: A review of fabrication techniques, Solid-State Electron. **26**(3), 179–197 (1983)

9.63 H. H. Berger: Models for contacts to planar devices, Solid-State Electron. **15**, 145–158 (1972)

9.64 R. H. Cox, H. Strack: Ohmic contacts for GaAs devices, Solid-State Electron. **10**, 1213–1218 (1967)

9.65 P. W. Debye: *Polar Molecules* (Chemical Catalog, New York 1927)

9.66 C. P. Smyth: *Dielectric Behavior and Structure* (McGraw Hill, New York 1955)

9.67 K. S. Cole, R. H. Cole: Absorption in dielectrics dispersion, J. Chem. Phys. **9**, 341 (1941)

9.68 H. Fröhlich: *Theory of Dielectrics* (Oxford Univ. Press, Oxford 1949)

9.69 N. Hill, W. E. Vaughman, A. H. Price, M. M. Davies: *Dielectric Properties and Molecular Behavior* (Van Nostrand Reinhold, New York 1969)

9.70 C. J. F. Bottcher, P. Bordewijk: *Theory of Electric Polarization* (Elsevier, New York 1996)

9.71 N. G. McCrum, B. E. Read, G. Williams: *Anelastic and Dielectric Effects in Polymeric Solids* (Wiley, New York 1967)

9.72 J. P. Runt, J. J. Fitzgerald: *Dielectric Spectroscopy of Polymeric Materials* (Am. Chem. Soc., Washington 1997)

9.73 D. W. Davies: *The Theory of the Electric and Magnetic Properties of Molecules* (Wiley, New York 1969)

9.74 A. R. von Hippel (ed.): *Dielectric Materials Applications* (Wiley, New York 1954)

9.75 H. E. Bussey: Measurement of RF properties of materials, A survey, Proc. IEEE **55**(5), 1046–1053 (1967)

9.76 S. O. Nelson: Dielectric properties of agricultural products, IEEE Trans. El. Insul. **26**, 845–869 (1991)

9.77 A. W. Kraszewski, S. Trabelsi, S. O. Nelson: Broadband microwave wheat permittivity meaurements in free space, J. Microwave Power Electromag. Energy **37**, 41–54 (2002)

9.78 F. Kremer, A. Schönhals: *Broadband Dielectric Spectroscopy* (Springer-Verlag, Berlin, Heidelberg 2003)

9.79 J. C. Maxwell: *An Elementary Treatise on Electricity*, 2nd edn. (Clarendon, Oxford 1888)

9.80 S. Havriliak, S. J. Negami: A complex plane analysis of α-dispersions in some polymer systems, J. Polym. Sci. C: Polym. Symp. **14**, 99 (1966)

9.81 D. W. Davidson, R. H. Cole: Dielectric relaxation in glicerine, J. Chem. Phys. **18**, 1417 (1950)

9.82 V. V. Novikov, V. P. Privalko: Temporal fractal model for the anomalous dielectric relaxation of inhomogeneous media with chaotic structure, Phys. Rev. E **64**, 031504 (2001)

9.83 V. V. Daniel: *Dielectric Relaxation* (Academic, London 1967)

9.84 A. K. Jonsher: *Dielectric Relaxation in Solids* (Chelsea Dielectrics, London 1983)

9.85 F. Alvarez, A. Alegria, J. Colmenero: A new method for obtaining distribution of relaxation times from frequency relaxation spectra, J. Chem. Phys. **103**, 798–806 (1995)

9.86 H. Schäfer, E. Sternin, R. Stannarius, M. Arndt, F. Kremer: Novel approach to the analysis of broadband dielectric spectra, Phys. Rev. Lett. **76**, 2177–2180 (1996)

9.87 L. Hartshorn, W. H. Ward: The measurement of the permittivity and power factor of dielectrics from 10^4 to 10^8 cycles per second, J. Inst. Electr. Eng. **79**, 567–609 (1936)

9.88 Agilent Technologies: *Accessories Selection Guide For Impedance Measurements, Dielectric Test Fixtures* (Agilent Technologies, Palo Alto 2001) p. 38 www.agilent.com

9.89 Application Note 1369-1: *Agilent Solutions for Measuring Permittivity and Permeability with LCR Meters and Impedance Analyzers* (Agilent Technologies, Palo Alto 2001) www.agilent.com

9.90 ASTM D 150-98: *Standard Test Method for AC Loss Characteristics and Permittivity of Solid Electrical Insulating Materials* (ASTM, West Conshohocken 1998) www.astm.org

9.91 D. A. Gray: *Handbook of Coaxial Microwave Measurements* (General Radio, West Concord. 1968)

9.92 S. Ramo, J. R. Whinnery, T. Van Duzer: *Fields and Waves in Communication Electronics* (Wiley, New York 1994)

9.93 Agilent Technologies: *RF and Microwave Test Accessories* (Agilent Technologies, Palo Alto 2006) www.agilent.com

9.94 J. P. Grant, R. N. Clarke, G. T. Symm, N. Spyrou: Acritical study of the open-ended coaxial line sensor technique for RF and microwave complex permittivity measurements, J. Phys. E Sci. Instrum. **22**, 757–770 (1989)

9.95 Agilent Technologies: *85070C Dielectric Probe Kit* (Agilent Technologies, Palo Alto 2005) www.agilent.com

9.96 M.A. Stuchly, S.S. Stuchly: Coaxial line reflection methods for measuring dielectric properties of biological substances at radio and microwave frequencies: A review, IEEE Trans. Instrum. Meas **29**, 176–183 (1980)

9.97 M.F. Iskander, S.S. Stuchly: Fringing field effect in the lumped-capacitance method for permittivity measurements, IEEE Trans. Instrum. Meas **27**, 107–109 (1978)

9.98 J.K. Hunton: Analysis of microwave techniques by means of signal flow graphs, IRE Trans. Microwave Theory Tech. **8**, 206–212 (1960)

9.99 K. Kurokawa: Power waves and the scattering matrix, IEEE Trans. Microwave Theory Tech. **13**, 194–202 (1965)

9.100 A. M. Nicolson: Broad-band microwave transmission characteristics from a single measuramant of the transient response, IEEE Trans. Instrum. Meas. **19**, 337–382 (1970)

9.101 S.S. Stuchly, M. Matuszewski: A combined total reflection-transmission method in application to dielectric spectroscopy, IEEE Trans. Instrum. Meas **27**, 285–288 (1978)

9.102 Product Note 8510-3: *Measuring the dielectric constant of solids with the HP network analyzer* (Hewlett Packard, Palo Alto 1985)

9.103 J. Baker-Jarvis, R.G. Geyer, P.D. Domich: A nonlinear least-squares with causality constraints applied to transmission line permittivity, IEEE Trans. Intrum. Meas **41**, 646–652 (1992)

9.104 J. Obrzut, A. Anopchenko: Input impedance of a coaxial line terminated with a complex gap capacitance – numerical experimental analysis, IEEE Trans. Instrum. Meas **53**, 1197–1202 (2004)

9.105 Institute for Printed Circuits: *Standard Test Method Manual, TM-650, Method 2.5.5.10, High frequency testing to determine permittivity and loss tangent of embedded passive materials* (IPC, Bannockburn 2005) www.ipc.org

9.106 ASTM D2520-01: *Standard Test Methods for Complex Permittivity (Dielectric Constant) of Solid Electrical Insulating Materials at Microwave Frequencies and Temperatures to 1650 °C, Test method B-Resonant Cavity Perturbation Method* (ASTM, West Conshohocken 1998) www.astm.org

9.107 G. Kent: Nondestructive permittivity measurements of substrates, IEEE Trans. Instrum. Meas. **45**, 102–106 (1996)

9.108 S. Maj, M. Pospieszalski: Acomposite multilayered cylindrical dielectric resonator, IEEE MTT-S Digest, 190–192 (1984)

9.109 J. Krupka, K. Derzakowski, A. Abramowicz, M.E. Tobar, R.G. Geyer: Use of whispering-gallery modes for complex permittivity determinations of ultra-low-loss dielectric materials, IEEE Trans. Microwave Theory Tech. **47**, 752–759 (1999)

9.110 G.I. Woolaver: Accurately measure dielectric constant of soft substrates, Microwave and RF **24**, 153–158 (1990)

9.111 S.S. Stuchly, M.A. Rzepecka, M.F. Iskander: Permittivity measurements at microwave frequencies using lumped elements, IEEE Trans Instr. Meas **23**, 56–62 (1974)